JGR Oceans

RESEARCH ARTICLE
10.1029/2019JC014982

Inferring Air-Sea Carbon Dioxide Transfer Velocities From Sea Surface Scatterometer Measurements

M. Ghobadian[1] and D. Stammer[1]

[1]Centrum für Erdsystemforschung und Nachhaltigkeit, Universität Hamburg, Hamburg, Germany

Key Points:
- Derivation of new air-sea flux parameterization for CO_2 fluxes
- Application of new parameterization to satellite scatterometer data
- Provision of seasonal and annual mean CO_2 estimates

Correspondence to:
D. Stammer,
detlef.stammer@uni-hamburg.de

Citation:
Ghobadian, M., & Stammer, D. (2019). Inferring air-sea carbon dioxide transfer velocities from sea surface scatterometer measurements. *Journal of Geophysical Research: Oceans*, *124*, 7974–7988. https://doi.org/10.1029/2019JC014982

Received 30 JAN 2019
Accepted 30 SEP 2019
Accepted article online 17 OCT 2019
Published online 19 NOV 2019

Abstract C-band microwave sea surface radar backscatter observations from the FINO-2 tower in the western Baltic are analyzed with respect to their relevance for air-sea CO_2 transfer velocity parameterizations. The scatterometer measurements observed from a height of 25 m above the sea surface using a multifrequency scatterometer instrument of the University of Hamburg were obtained quasi-simultaneously with eddy covariance CO_2 flux measurements. Both data sets are merged here to derive a gas transfer velocity parameterization based on radar backscatter measurements. At the location of the FINO-2 tower, the resulting time-averaged gas transfer velocity amounts to 26.95 cm/hr. In combination with ΔP_{CO_2} measurements available from the vicinity of the FINO-2 platform, a time-mean CO_2 flux of 0.23 $\mu mol \cdot m^{-2} \cdot s^{-1}$ into the Baltic was estimated. Applied to monthly mean satellite-based C-band ASCAT scatterometer data, the newly derived gas transfer velocity parameterization provides estimates of seasonal and annual mean global maps of air-sea transfer velocities. The new results agree in their general pattern with previous estimates using wind speed parameterization. However, the backscatter-based transfer velocities appear smaller at higher latitudes. Globally averaged air-sea CO_2 fluxes would thereby be reduced by 20%. To what extent this is a robust result, or if it depends on the fact that the training data set did not represent conditions, has to be investigated in the future.

1. Introduction

Air-sea gas exchange processes play an important role in climate change since they are the controlling mechanism for the uptake of anthropogenic CO_2 by the ocean. Without this uptake, about 25% more anthropogenic CO_2 concentration would exist in the atmosphere with severe consequences for global temperature rise (Pachauri et al., 2014). Quantifying the ongoing air-sea gas flux and monitoring the ocean sink of anthropogenic carbon, therefore, is key for better projections of global warming. But although air-sea fluxes of CO_2 have been studied for many decades, considerable uncertainties remain in existing time-mean estimates (Jonsson et al., 2008; Lansø et al., 2015; Takahashi et al., 2002; Yu et al., 2014). It is conceivable that uncertainties are even larger for the time-varying flux component. For a better quantification of the oceanic CO_2 uptake, both uncertainties have to be reduced.

In general terms, the air-sea flux of CO_2 can be expressed as

$$F = \alpha \, \kappa \, \left(P_{CO_{2,water}} - P_{CO_{2,air}} \right), \tag{1}$$

where κ represents the gas transfer velocity (in cm/hr), α the solubility of gas in seawater (in $mol \cdot m^{-3} \cdot atm^{-1}$), and $(P_{CO_{2,water}} - P_{CO_{2,air}})$ stands for the partial pressure difference between seawater and the air above (in μatm), henceforth referred to as ΔP_{CO_2}. According to equation (1), the CO_2 flux depends linearly on κ and ΔP_{CO_2}. To reduce uncertainties in the time-varying air-sea fluxes of CO_2, we therefore need to improve estimates of these two parameters as a function of space and time. This holds especially for parameterizations of the transfer velocity κ, which typically is described as a function of large-scale observable parameters.

Among the most common gas transfer velocity parameterizations are empirical relations with wind speed at 10 m height (e.g., Ho et al., 2006; Liss & Merlivat, 1986; Nightingale et al., 2000; Wanninkhof, 1992; Wanninkhof & McGillis, 1999; Wanninkhof et al., 2009) because wind controls air-sea gas exchange through its influence on the surface waves and especially turbulence and wind speed near the ocean surface can be used as a proxy to estimate gas transfer velocity. The resulting traditional wind-based parameterization of gas transfer velocity is of the form

$$\kappa = a \, (U/U_0)^b \, (Sc)^n, \tag{2}$$

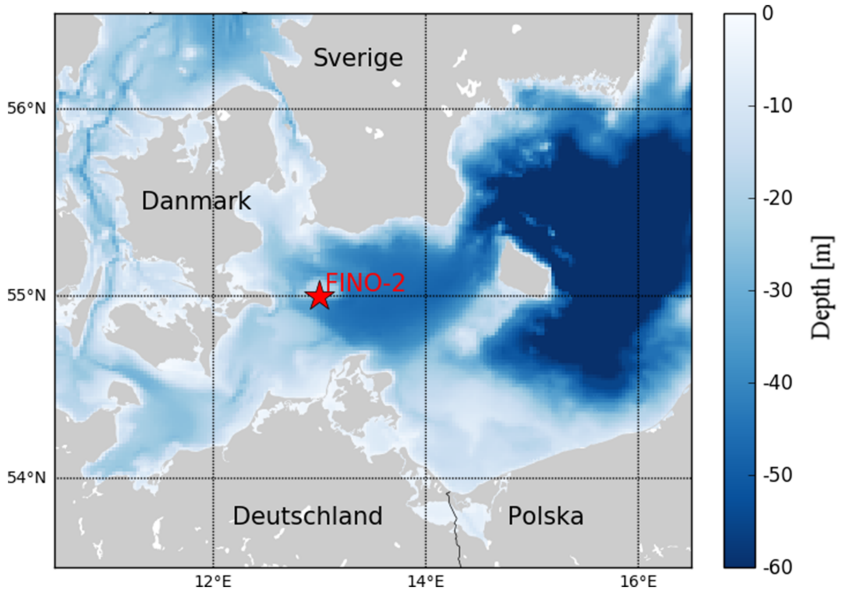

Figure 1. Experimental site in the Western Baltic Sea. Shown is the bottom iowtopo2 topography (in m). The red star mark the location of the FINO-2 tower.

where U is the wind speed at 10 m height above sea level, $U_0 = 1$ m/s, a (in cm/hr) and b are coefficients determined by experimental data, Sc is the Schmidt number, and the exponent n is an empirical value which varies between one half and two thirds depending on the friction velocity and mean square slope of the surface waves (Jähne et al., 1989). However, several processes other than just wind speed mediate air-sea fluxes as well, such as surface films or wave breaking which are difficult to account for in wind speed parameterization (Broecker et al., 1978; Merlivat & Memery, 1983). Equation (2) is therefore not a sufficient descriptor of all factors or physical processes involved (Banner & Phillips, 1974; Bock et al., 1999; Melville, 1996; Weiss et al., 2007). Takahashi et al. (2002) quantified this uncertainty as variation in the global oceanic CO_2 uptake of 50% or more as a consequence of the different wind exponents in the regional gas transfer velocity parameterizations that account for these difficulties.

In this paper we attempt to improve estimates of the time-varying gas transfer velocity parameterizations, κ. Improvements will be sought by using surface roughness as the primary controlling observable; because of the strong dependence of transfer velocity on small-scale turbulence and wave breaking, surface roughness or surface wind stress should be a better proxy for estimating surface CO_2 transfer as compared to one dependent only on wind speed. An effective way to estimate small-scale surface roughness can be accomplished using radar backscatter measurements from the sea surface as measured by radar instruments from space. It therefore appears to be an important step to test the usefulness of such globally recorded radar backscatter data for estimates of surface CO_2 fluxes over the global ocean as a function of time and geographic position. First respective approaches were investigated by Glover et al. (2002) based on altimetric data sets. Building on these earlier results, here we analyze the usefulness of radar cross-section measurements as input for a new κ parameterization which intrinsically takes into account various environmental forcing mechanisms. The study is based on multipolarization scatterometer observations obtained in the C-band (5.3 GHz) at incidence angles of 35°, 45°, and 55° in the western Baltic. The resulting new κ parameterization will then be transferred and applied to global satellite-based C-band scatterometer sets to obtain new global estimates of time-varying air-sea CO_2 gas fluxes.

The remaining paper is structured as follows: Section 2 describes the methodology and the experimental data from the Western Baltic Sea. Section 3 presents a new backscatter-based CO_2 flux parameterization derived from scatterometer data. Its pilot application to the satellite scatterometer data to obtain new estimates of global gas CO_2 fluxes will be discussed in section 4, followed by concluding remarks in section 5.

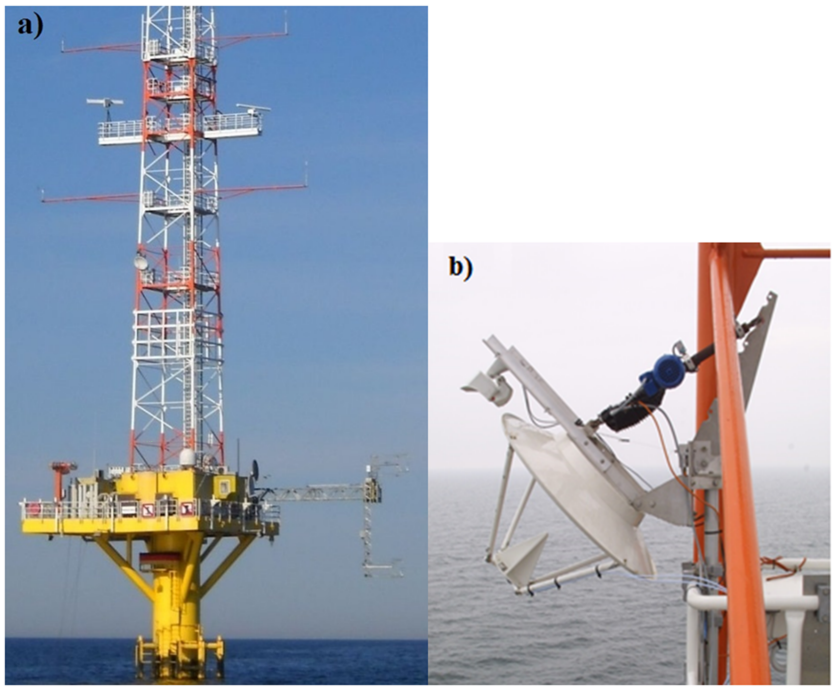

Figure 2. (a) The research platform FINO-2 on which the scatterometer antenna was mounted at a height of 25 m above the sea surface. (b) The Multi3Scat antenna. Pictures taken by Mayk Fischer.

2. Methodology

Our study is based on C-band surface roughness measurements obtained on the German research platform FINO-2 using a microwave scatterometer. The research platform is located in the western Baltic, 35 km north of the Island Rügen at a water depth of 54 m (Figure 1). The experimental setup is illustrated in Figure 2, showing in its left panel the FINO-2 tower on which the scatterometer antenna was mounted pointing in a westward direction (Figure 2b). Several other sensors also present on the FINO-2 platform measured wind speed and direction, air temperature, air pressure, solar radiation, atmospheric humidity, and precipitation, at different heights from 30 to 100 m, every 10 m. Also collected near the platform were observations of water surface temperatures, wind, and wave parameters. The sea surface temperature and significant wave height (SWH) were measured by a buoy about 150 m away from the platform and provided data points every 30 min.

2.1. Scatterometer Observation of Sea Surface

The radar backscatter measurements were carried out as part of the German SOPARN project during a 27-month period from 2011 to 2013 using the multifrequency and multipolarization scatterometer

Table 1
Technical Specification of the Multi3Scat Instrument

Type	Doppler scatterometer					
Antenna	Dual polarized parabolic antenna					
Microwave bands	L	S	C	X	Ku	
Frequency (GHz)	1.0	2.4	5.3	10.0	15.0	
Wavelength (cm)	30.0	12.5	5.7	3.0	2.0	
Gain (dBi)	14	22	28	33	35	
3 dB beamwidth (°)	22	10	4.5	2.5	1.5	
	35°	83.3	13.8	2.7	0.79	0.33
Footprint (m^2)	45°	132.6	21.6	4.3	1.2	0.51
	55°	260.8	40.8	8.15	2.29	0.96

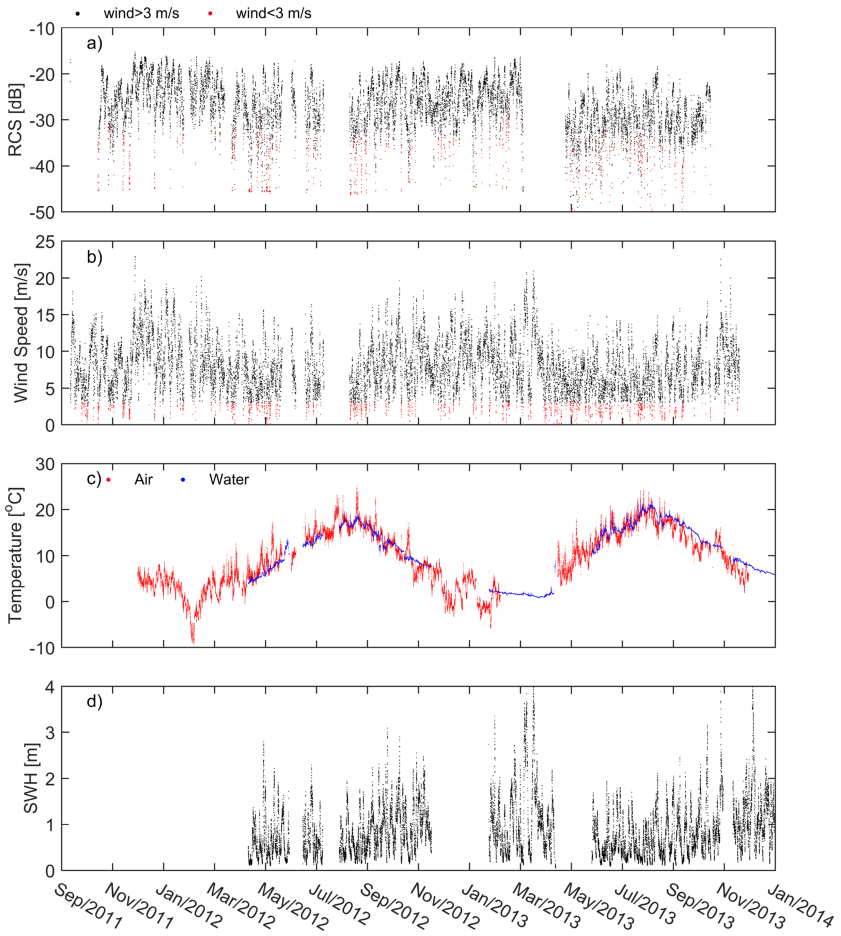

Figure 3. Time series of the data measured at the FINO-2 platform. Each point indicates a bin average representing 30 min of observations. (a) Radar backscatter at 5.3 GHz, VV polarization, and 55° incidence angle. The black dots correspond to backscattering at wind speed above 3 m/s; the red dots are the backscattering at wind speed below 3 m/s. (b) Wind speed over the entire measurement period with same color coding as above. (c) Water temperature measured in blue and air temperature extrapolated to the temperature at 10 m height in red. (d) Significant wave height.

Multi3Scat of the University of Hamburg. The scatterometer instrument consists of an antenna, a microwave unit, a control unit, a direct digital synthesizer module, and a data storage unit. The antenna was mounted with a fixed westward looking orientation because this is the prevailing wind direction at the platform location. The technical overview of the Multi3Scat is summarized in Table 1 (see also Kern et al., 2009, for a helicopter-based application of the instrument).

Measurements of radar backscatter were obtained at about 5 min intervals at five microwave bands L, S, C, X, and Ku (corresponding to 1.0, 2.3, 5.3, 10.0, and 15.0 GHz, respectively), in four polarization combinations (HH, HV, VV, and VH; the first and second letter denoting the polarization in horizontal [H] or vertical [V] directions of the transmitted and the received signal, respectively) and with three incidence angles (35°, 45°, and 55°). In this study the analysis is limited to the multipolarization C-band data because this corresponds in frequency to available satellite data. Because the two cross-polarized data sets are identical, only the VH polarized signal will be analyzed. And because the platform itself has a negative influence on the wind and thus on the surface roughness pattern, we will limit the analysis here to westward wind situations, that is, to upwind situations.

An example of the resulting C-band backscatter signal from the sea surface is shown in Figure 3a in the form of a time series of the radar backscatter observations received with VV polarization and an incidence angle 55° at different sea surface and weather conditions. The shown backscatter data are in agreement with previous findings (e.g., Jones & Schroeder, 1978; Keller et al., 1989; Plant et al., 1985); however, measurements become very noisy as soon as the wind speed declines below 3 m/s for which conditions the sea surface

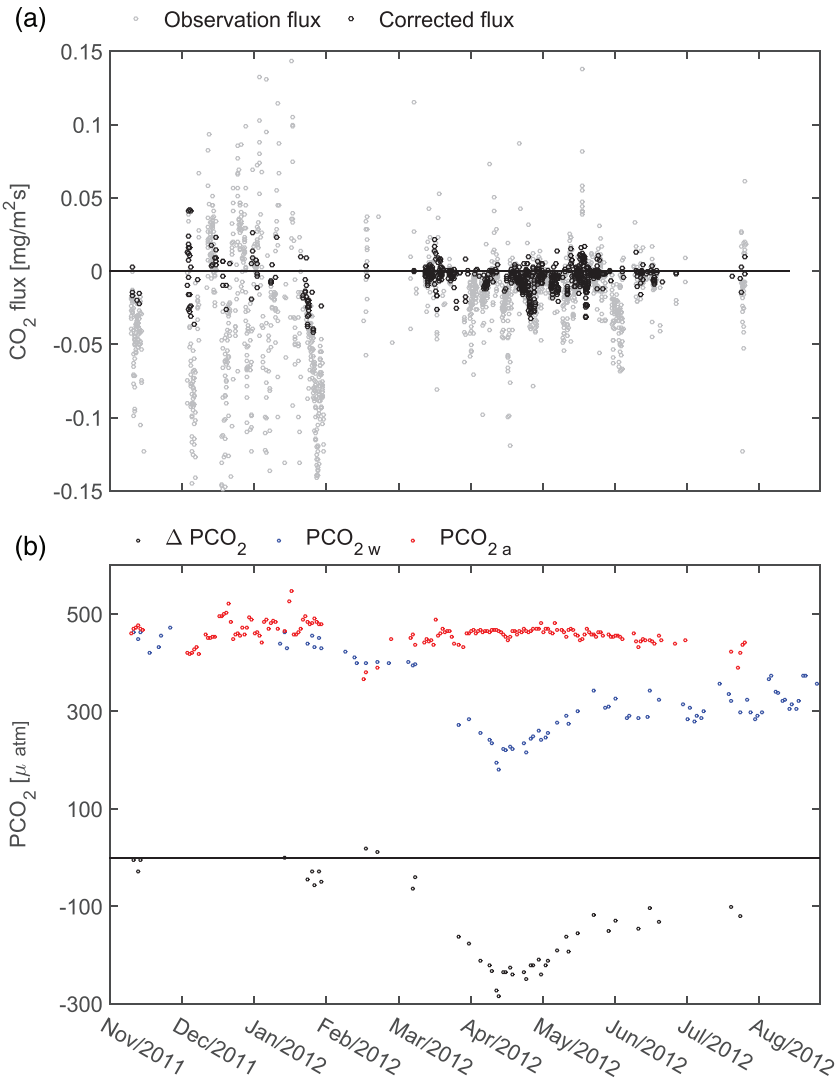

Figure 4. Time series of (a) hourly averaged CO_2 flux from eddy covariance system (gray) and corrected flux (black), and (b) partial pressure in the air and water surface, collected at the FINO-2 platform from November 2011 until August 2012.

becomes smoother (red dots in Figures 3a and 3b). These measurements were therefore eliminated from further analysis.

Shown in the remaining panels of the figure are time series of wind speed, air temperature, sea surface temperature, and SWH. Clearly seen from the figure is a seasonal signal showing higher backscatter values during winter time conditions and lower values during the summer, in agreement with respective modulations of the wind stress. Stronger winds are present from October to February, and weaker wind are observed from April to June. The bulk of the measurements was obtained for moderate wind speeds between 5 to 10 m/s; only occasionally were values above 20 m/s reached (cf. the top two panels). Horizontal currents (not shown) are weak near the FINO-2 platform (about 10 cm/s), and the sea surface temperature typically varies between 10° and 25° (Figure 3c). Amplitudes of SWH were typically found between 0.5 to 1.5 m (Figure 3d); associated wave periods of about 7 to 8 s are relatively short except during strong storms.

2.2. CO_2 Transfer Velocity Derived From Eddy Covariance Observations

Mounted on the FINO-2 platform was also an eddy covariance setup producing CO_2 flux estimates quasi-simultaneous to the Multi3Scat measurements. The setup consisted of a three-component sonic anemometers (USA1) and an open-path infrared gas analyzer (LICOR 7500) for CO_2 and H_2O. These instruments were operated on a 9 m long boom pointing southward from the platform at heights of 6.8 and

13.8 m above the sea surface, respectively. The open-path infrared gas analyzer provided measurements of the densities of carbon dioxide and water vapor in turbulent air structures with a resolution of 10 Hz. Based on the eddy covariance technique, these data were used in conjunction with sonic anemometer air turbulence data to determine the fluxes of CO_2 and H_2O integrated over 30 min intervals. The eddy covariance measurements were performed from November 2011 until August 2012, as described by Lammert and Ament (2015).

Additional water P_{CO_2} measurements were obtained from cargo ships moving along a transect between Helsinki in the Gulf of Finland and Lübeck/Gdynia in the southwest of the Baltic Sea (Schneider et al., 2014). These P_{CO_2} measurements were obtained via equilibration of surface water with air and subsequent detection of the equilibrium CO_2 concentration using infrared spectroscopy as described by Schneider et al. (2014). Combined with the eddy covariance data, the ship-based measurements provided estimates of partial pressure differences of CO_2 in the air and seawater.

Figure 4 shows the resulting daily averaged CO_2 flux time series (top panel), together with time series of the partial pressure differences of CO_2 in the air and seawater during 2011 and 2012 (bottom panel). During March, the surface water P_{CO_2} drops, presumably as a result of intensive primary production. The increase from there toward summer P_{CO_2} values can be rationalized by the temperature solubility effect on P_{CO_2} in the water. CO_2 fluxes are maximum during winter time when they reach values of up to 0.15 $mg \cdot m^{-2} \cdot s^{-1}$ from the atmosphere into the ocean. Because these enhanced CO_2 fluxes occur in the presence of weak air-sea P_{CO_2} difference (see bottom panel), they need to be associated with enhanced gas transfer velocities, κ, resulting from enhanced surface wind speeds and an associated sea surface roughness. A detailed investigation of the P_{CO_2} in the Baltic Sea can be found in Schneider et al. (2009).

As can be seen from the figure, the estimates of winter CO_2 fluxes are extremely noisy due to random errors in atmospheric P_{CO_2} measurements (Lammert & Ament, 2015). To reduce this noise, we exclude all flux data exceeding the range of one monthly standard deviation of the individual 30 min data points. Mean and standard deviations were computed for each month individually over the observational period, thereby accounting for the seasonal variations in the mean. The gas analyzer counts the number of CO_2 molecules in the sample air volume, it therefore determines the density of CO_2 but not the mixing ratio. Moreover, the turbulent CO_2 flux determined by the eddy covariance system from the CO_2 density fluctuations is affected by fluctuations in air temperature and air pressure, as well as H_2O density fluctuations. Eddy covariance flux measurements therefore need to be corrected for density fluctuations not related to air-sea gas exchange. For this purpose, a Webb-Pearman-Leuning density correction (Webb et al., 1980) was applied to the FINO-2 eddy covariance measurements. While usually small, in some cases, the correction can be of the same order as the turbulent flux itself; then the density correction of Webb would not be a sufficient correction for all CO_2 flux values. To test this, we compare the flux velocity of CO_2 to that of heat and water vapor, as suggested by Weiss et al. (2007). Upon this test, any CO_2 flux data with flux velocities higher than 10 times the flux velocities of heat flux measured simultaneous to the CO_2 flux where eliminated. For further details, see Lammert and Ament (2015).

Based on the corrected eddy covariance flux time series also shown in Figure 4a, we can infer the underlying gas transfer velocity, κ, from the eddy covariance data using equation (1), as

$$\kappa = \frac{F_{CO_2}}{\alpha \Delta P_{CO_2}}. \tag{3}$$

To compare our resulting transfer velocity κ with published methods, it needs to be converted into the normalized transfer velocity, κ_{660}, as

$$\kappa_{660} = \kappa \left(\frac{Sc}{660}\right)^{-0.5}. \tag{4}$$

Here, *Sc* is the Schmidt number that depends on the kinematic viscosity and molecular diffusivity as proposed by Wanninkhof (1992) and 660 corresponds to the CO_2 Schmidt number for seawater at a temperature of 20 °C.

We calculated the Schmidt number for this normalization using simultaneous salinity and surface temperature measurements from the Western Baltic Sea following Wanninkhof (1992) and using the coefficients

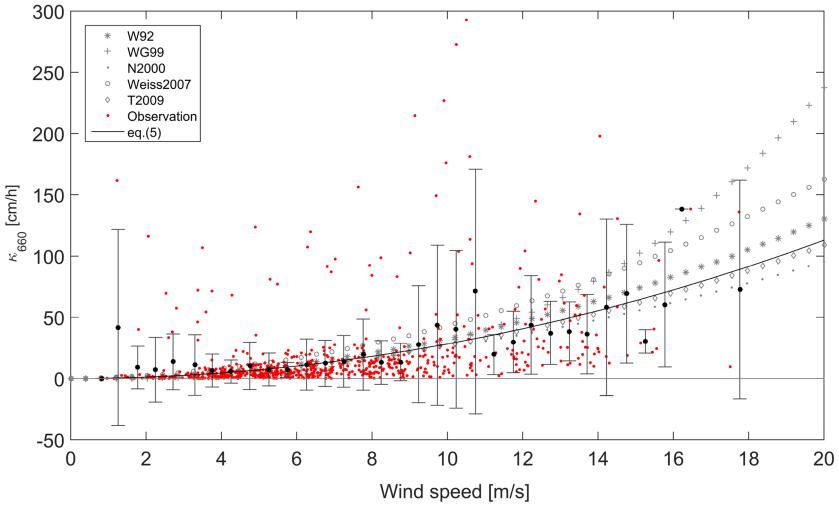

Figure 5. CO_2 transfer velocity cm/hr normalized with *Sc* number versus wind speed, from direct eddy covariance measurements (red dots). The averaged values of transfer velocity over 0.5 m/s classes of wind speed are shown in black bullets. The error bars correspond to standard deviations of each window. The curves with gray patterns describe model results of Wanninkhof (1992) (star), Wanninkhof and McGillis (1999) (plus), Nightingale et al. (2000) (dot), Weiss et al. (2007) (circle), and Takahashi et al. (2009) (diamond).

provided there. Figure 5 shows the resulting CO_2 transfer velocity κ_{660} for the western Baltic Sea, as a function of wind speed, representing the entire 10-month period from November 2011 to August 2012. Values reach up to 120 cm/hr for wind speed of 20 m/s. We recall, however, that 80% of these transfer velocity values were obtained at wind speeds below 10 m/s and that the interval between 100 and 300 cm/hr contains less than 5% of the total number of data points. Nevertheless, we can compare results to those using traditional parameterizations. To this end, the data were fit to a quadratic function of wind speed, leading to a coefficient of 0.28.

$$\kappa_{660} = 0.28 \cdot (U/U_0)^2 \quad \text{cm/hr}. \tag{5}$$

Here U is the wind at 10 m elevation above sea level and $U_0 = 1$ m/s. The correlation coefficient between the fitted line and the original data points is 0.63; using any other exponent (e.g., linear or cubic) would lead to a smaller correlation. The coefficient of the gas transfer parameterization of 0.28 shows close agreement with findings from Takahashi et al. (2009) (0.26) and Wanninkhof (1992) (0.31). Overall, our fitted curve lies between those from Takahashi et al. (2009) and Wanninkhof (1992).

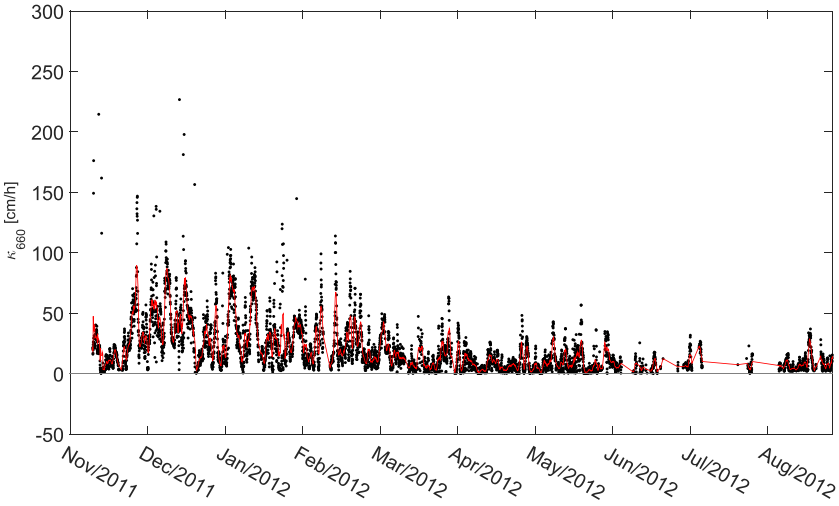

Figure 6. Time series of the CO_2 transfer velocity cm/hr normalized by the *Sc* number from direct eddy covariance measurements (black dots). The red curve describes the 12 hr moving mean.

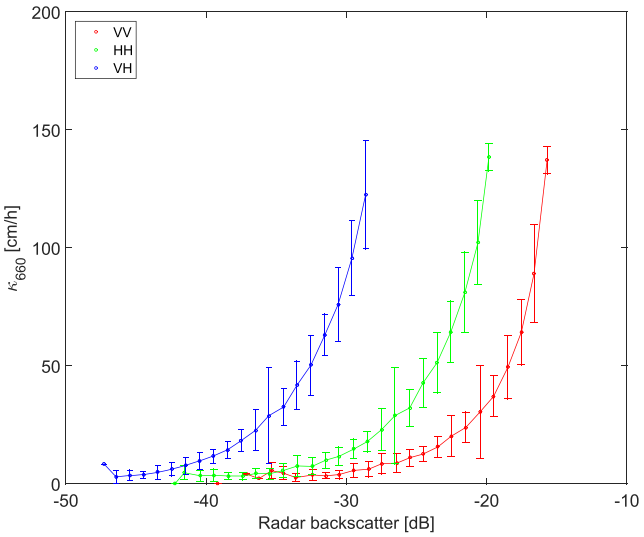

Figure 7. Upwind C-band radar backscatter from Multi3Scat observations versus gas transfer velocity computed from the direct eddy covariance observations, both in the Western Baltic Sea. The data are averaged over the period from November 2011 to August 2012, providing one data point every 1 m/s wind speed. Red, green, and blue correspond VV, HH, and VH polarization radar backscatter, respectively. The error bars represent one standard deviation of the uncertainty.

In comparison to traditional transfer velocity parameterizations (also included in the figure), all results appear to agree mostly for wind speeds below 10 m/s. However, differences become prominent for larger wind speeds, especially with respect to Wanninkhof and McGillis (1999) and Weiss et al. (2007). In an root-mean-square difference sense, our findings are closest to the gas transfer velocity of Nightingale et al. (2000) with a root-mean-square difference of 10 cm/hr and a correlation coefficient of 0.89, followed by the parameterization of Wanninkhof (1992) with nearly the same root-mean-square difference and correlation coefficient. For Weiss et al. (2007) and Wanninkhof and McGillis (1999), the root-mean-square differences reach values of about 14 and 19 cm/hr, respectively.

A time series of the transfer velocity κ_{660} reveals its strong seasonal variation likely results from changes in the wind-induced turbulence (Figure 6). Enhanced κ_{660} values occur during winter months and substantially reduced transfer velocities during summer time. In contrast, the stress at the surface potentially is enhanced during spring due to reduced atmospheric stability.

The seasonality in κ_{660} suggests that a relation like equation (5) should be derived as a function of season. In our case, such a seasonally dependent relation between the gas transfer velocity and wind speed varies the coefficient of equation (5) from 0.11 for winter and autumn and 0.42 for summer and spring, that is, by about a factor of 4; a fact that could have a strong impact on global estimates of CO_2 fluxes. We do note that a backscatter-based parameterization would already account for such a seasonality as the backscatter is affected by all relevant processes.

3. Backscatter-Based CO_2 Flux Parameterization

The goal of this paper is to derive a κ_{660} parameterization in the form of surface radar backscatter dependence. Shown in Figure 7 is an empirical relation between the upwind C-band radar backscatter measurements and the simultaneous eddy covariance based κ_{660} gas transfer velocity shown in Figure 6. Figure 7 shows the relations separately for VV (red), HH (green), and VH (blue) polarizations. For each polarization, valid data pairs were binned in 1 dB intervals, and the means are plotted for each bin connected by a line with the bin-STD superimposed as error bars. Only scatterometer data that overlap in time with the eddy covariance observation from November 2011 to August 2012 are used in this analysis. The figure reveals the differences in κ_{660} dependencies on the VV, HH, and VH radar backscatter data, which can be rationalized by the different impacts of surface processes such as Bragg scattering, wave breaking, or steep waveforms on backscatter in each polarization.

Fitting a power law to each resulting mean value leads to an empirical relationship between κ_{660} and the upwind backscatter for each microwave frequency band and polarization pq (i.e., VV, HH, and VH), respectively, in the form of

$$\kappa = A \cdot \sigma_{pq}^{B}. \tag{6}$$

Table 2
Empirically Coefficients of the Scatterometer Retrieved Gas Transfer Velocity From the Experiments by the Multi3Scat at C-Band Radar Frequency and Different Polarizations and Their Related Statistics

$\kappa = A \cdot \sigma_{pp}^{B}$					
Setting		A (cm/hr)	B	RMSE (cm/hr)	r
C-band	VV	6, 516	1.1	10.05	0.90
	HH	9, 332	0.9	9.70	0.91
	VH	50, 234	0.9	9.29	0.92

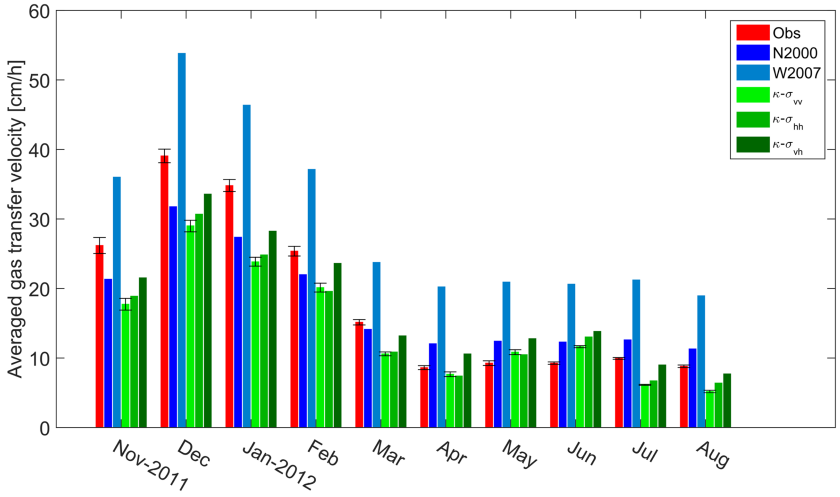

Figure 8. Seasonal variation of the averaged gas transfer velocity in the Western Baltic Sea. The panel shows in red observational gas transfer velocity, in blue and turquoise the wind-based gas transfer velocities of Nightingale et al. (2000) and Weiss et al. (2007), respectively, and in green colors the scatterometer-based gas transfer velocity.

Here σ_{pq} has logarithmic values with units of dB. The coefficient A has units of cm/hr. All respective empirically determined coefficients A and B of the scatterometer-based gas transfer velocities obtained from the Multi3Scat observations are shown in Table 2 for C-band at all polarizations. Also summarized are the root-mean-square differences and correlation coefficients. It can be seen from the table that HH polarization leads to better agreement as compared to VV, with smaller root-mean-square error and better correlation coefficient r.

With the results at hand, we can now summarize the seasonal cycle present in transfer velocity κ_{660} at the FINO-2 location. To this end, we computed the climatological monthly means from the scatterometer-based gas transfer velocities and compared them with the monthly mean values of the transfer velocity observed through the eddy covariance method. Results are plotted in Figure 8 and confirm that the largest gas transfer velocity values exist during the winter season from November to January and the smallest in April and August. We note that, except in May, the transfer velocities computed from radar backscatter data are smaller in value than those observed. In contrast, the wind-based model of Nightingale et al. (2000) (labeled N2000 in the figure) produces smaller values than observations in all cold months and larger values than observations in all warm months, except March. Finally, the model of Weiss et al. (2007) (labeled W2007 in the figure) produces particularly large overestimation at high wind speed (the light blue bars). We also note that during the cold season, HH backscatter retrieved gas transfer velocity is better correlated with observations, while during stable atmospheric conditions and small-scale wave breaking and surface roughness, VV backscatter correlates better with the eddy covariance observations.

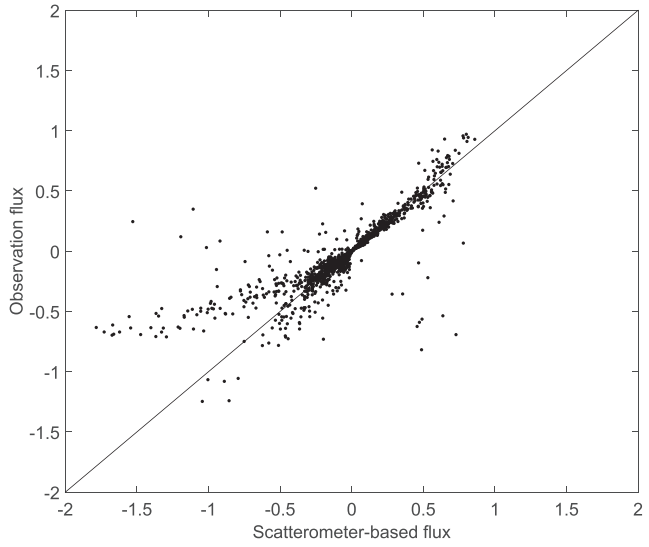

Figure 9. Scatter diagram of the CO_2 flux from observation in the Western Baltic Sea against the computed flux using microwave backscatter in the same area. The correlation between the two data sets is $r = 0.83$. Only a small offset about 0.027 $\mu mol \cdot m^{-2} \cdot s^{-1}$ can be detected.

Using ΔP_{CO_2} observations shown in Figure 4 and invoking equation (1), we computed the bulk surface CO_2 fluxes associated with the scatterometer-based κ_{660} time series (Figure 9). A comparison of the resulting fluxes with those obtained directly from the eddy covariance system (also shown in the figure) reveals a tight relation between both estimates in the range above -0.5 $\mu mol \cdot m^{-2} \cdot s^{-1}$. The spread below results from a cutoff in eddy covariance observations due to instrumental drifts or biases due to thermal expansion. Despite those differences for high negative magnitudes, the correlation between the two data sets is high ($r \sim 0.83$). Overall, only a small offset of about 0.027 $\mu mol \cdot m^{-2} \cdot s^{-1}$ can be detected across the entire range.

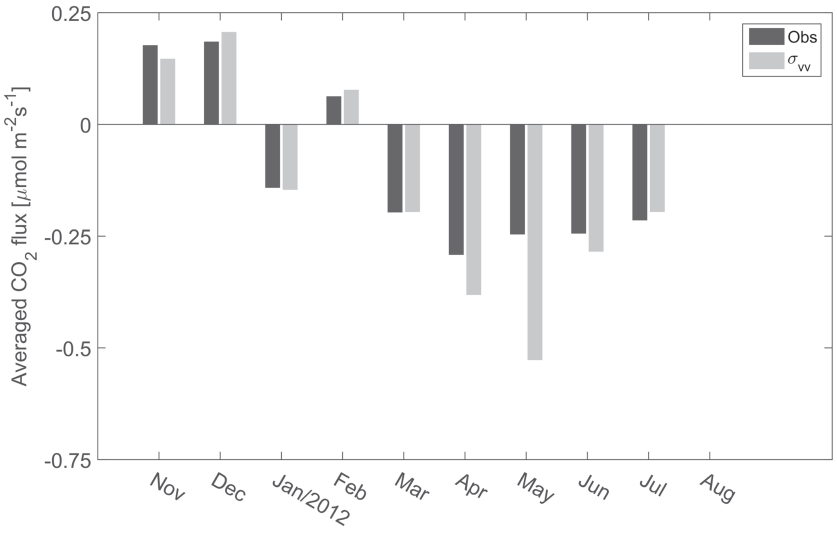

Figure 10. Seasonal variation of monthly averaged CO_2 flux in the Western Baltic Sea from the direct eddy covariance measurements (in dark gray) and the estimated flux using scatterometer data (in light gray).

As before for the transfer velocity, we can isolate the seasonal cycle also in the surface fluxes of CO_2 at the FINO-2 location (Figure 10). The figure compares the CO_2 fluxes obtained from the eddy covariance system with those computed from the scatterometer observations at C-band, VV polarization. A good agreement between both estimates is obvious, especially during the cold season. However, during summer months, the scatterometer-based estimates seem to overestimate the fluxes into the ocean during April and May due to the enhanced scatterometer-based κ_{660} during those months. During winter months, we can identify a CO_2 flux at the FINO-2 location from the ocean into the atmosphere when no primary productivity takes place in the water. In contrast, between May and August, the flux reverses when the primary productivity in the Baltic is large. It remains unclear, however, whether the negative values during January present in both estimates are an artifact and, if true, what could lead to such flux reversal during this month relative to the rest of the season.

4. Global Satellite Scatterometer-Based CO_2 Flux Estimates

Ultimately, a scatterometer-based κ_{660} parameterization should be applicable to satellite-based data sets to infer time-varying CO_2 fluxes over the global ocean. However, to be fully applicable, our parameterization inferred at the FINO-2 location would need to be tested at various other locations of the global ocean against in situ measurements. In the absence of such required data sets, we nevertheless test if such a step toward global time-varying estimates from satellite scatterometer is possible at all. To this end, we use, in a pilot setting, global space-borne vertically polarized advanced scatterometer (ASCAT) C-Band radar backscatter data, available during 2012 from the MetOp-B satellite (see www.eumetsat.int), to provide the first global maps of radar backscatter-based CO_2 flux fields.

We extracted the ASCAT data with spatial differences to the FINO-2 position of less than 0.05° and temporal differences relative to our scatterometer measurements of less than 60 min. For comparison we use the C-band, VV polarization, and incidence angles of 35°, 45°, and 55° from both data sources. Prior to the comparison, the backscatter data were grouped into specific ranges of wind direction for which a FINO-2-based algorithm exists and the Multi3Scat observations were averaged over 60 min for each incidence angle. From ASCAT, only data in upwind directions were used. In order to extract those satellite data relevant to the upwind direction, we combined the satellite track azimuth angle, beam azimuth angle, and wind direction. The wind direction for this purpose is computed from the Geophysical Model Function inversion which converts the sigma naught values to wind speed and direction.

The ASCAT instrument consists of two sets of three antennas. The radar beams are directed 45° forward, orthogonally, and 45° backward relative to the satellite's flight direction, on both sides of the satellite ground track. From the satellite track, we have the moving direction of the satellite. From the beam azimuth angle, we get the antenna side (left or right). Three values of sigma naught correspond to three antennas look

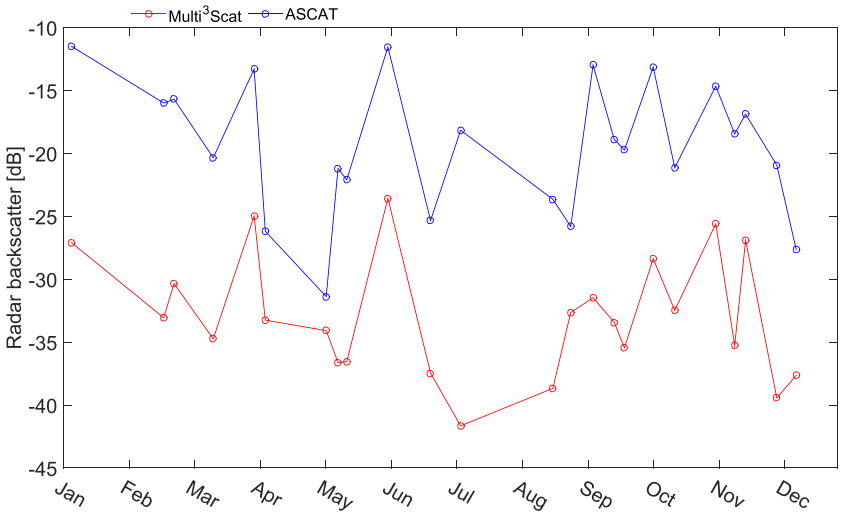

Figure 11. Platform-based radar backscatter measured by Multi3Scat compared to ASCAT radar backscatter from the same time (temporal difference of less than 1 hr) and location (spatial difference of less than 0.05°), in C-band, VV polarization, and upwind direction. A systematic bias about 13.5 dB is obvious.

angles with respect to the satellite track, which allow computing the antenna look direction. Combining this information with wind direction from ASCAT Level 2 products, we can extract the radar backscatter relevant for a particular azimuth angle. Azimuth angle is the horizontal angle between the wind and the antenna beam of the scatterometer. We collected upwind and downwind direction radar backscatter for gas transfer computation.

Figure 11 shows the comparison of the backscatter magnitudes of both data sets at the FINO-2 location, revealing similar temporal changes. To make the backscatter-based algorithm inferred from the Multi3Scat data applicable to the ASCAT data, the algorithm was adjusted for the apparent miscalibration of the Multi3Scat data by 13.5 dB before feeding the ASCAT data into the new gas transfer parameterization equation (6) with the A and B parameters as specified in Table 2 for the C-band and VV polarization. Shown in Figure 12 is a comparison of the respective gas transfer velocity estimates, revealing only a relatively small root-mean-square difference between both of 7.3 cm/hr and correlation coefficient of 0.81.

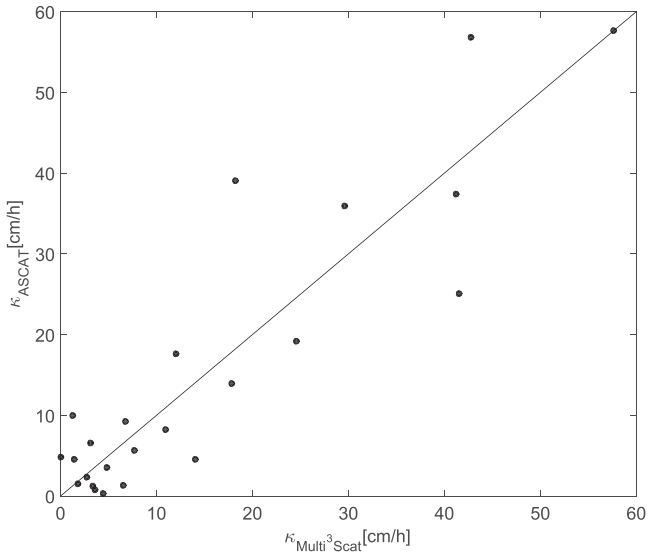

Figure 12. The retrieved transfer velocity from platform-based scatterometer data (Multi3Scat) versus ASCAT radar backscatter using our new parameterization. The RMS difference between both is 7.3 cm/hr; the correlation coefficient is $r = 0.81$.

Encouraged by this finding, we took the next step of applying the global ASCAT radar backscatter data to our new algorithm to produce maps of the global gas transfer velocity. To this end, we resampled ASCAT Global Data Service (GDS) Level 1 σ_0 fields on a 25 km Swath Grid. The data are available every 5 days along a swath of close to 1,000 km width. The ASCAT incidence angle ranges from 25° to 65°. Detailed information about the instrument, performance, calibration, processing, and generation of Levels 1 and 2 products of ASCAT are presented by EUMETSAT (2004, 2005, 2009a). The satellite track azimuth angle, beam azimuth angle, and wind direction provide an azimuth direction. Therefore, we collected upwind and downwind direction radar backscatter for gas transfer computation. The air-sea gas transfer velocity with respect to the azimuth direction and incidence angle was then computed for each satellite track using our new algorithm.

Global maps of resulting satellite-based air-sea CO_2 transfer velocity κ_{660} estimates are shown in Figure 13 on a 4° latitude and 5° longitude grid, separately for each season. The highest transfer velocities are found in high latitudes of both hemispheres during respective winter and autumn conditions there, while the lowest value resides on the equator because

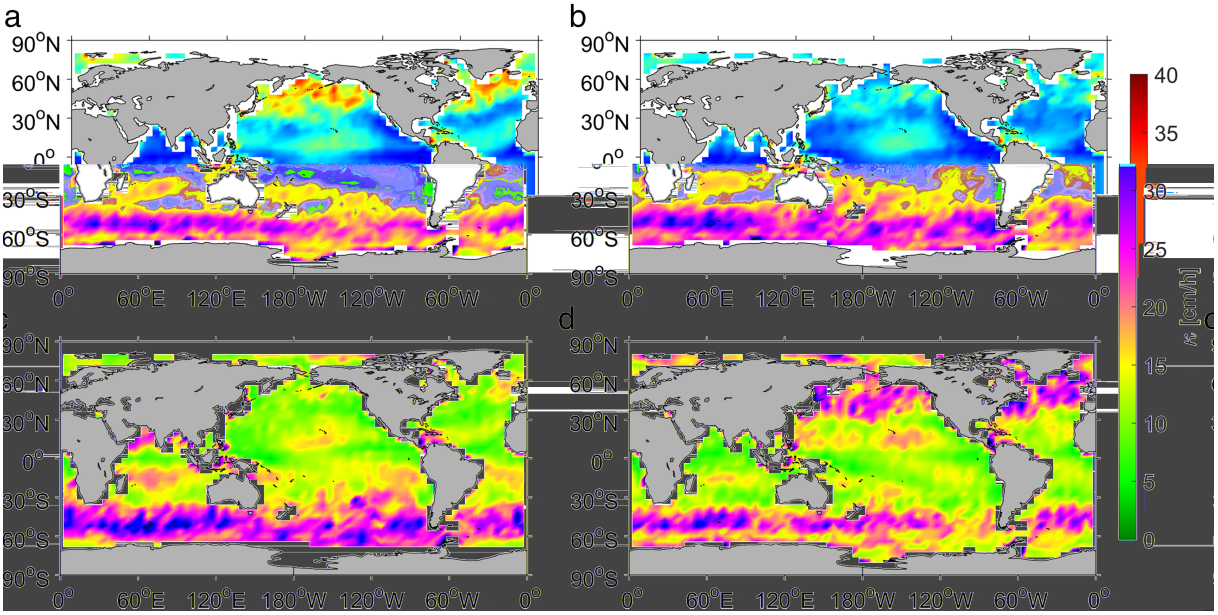

Figure 13. Estimates of global seasonal air-sea CO_2 transfer velocity derived from ASCAT satellite scatterometer using the new FINO-2-based algorithm. Shown are fields for (a) winter, (b) spring, (c) summer, and (d) fall.

of low wind speeds in this region. In autumn and winter, Northern Hemisphere midlatitudes show higher values than the other seasons. Similar patterns were reported previously by Wanninkhof (1992) from wind speed dependencies.

In a final step, air-sea CO_2 flux are calculated from equation (1) on the basis of the new transfer velocity parameterization using ASCAT radar backscatter data and monthly averaged ΔP_{CO_2} available from Takahashi et al. (2014). Climatological monthly mean ΔP_{CO_2} fields compiled on a 4° latitude and 5° longitude grid were retrieved from the LDEO database (NDP-094) at http://cdiac.ornl.gov/oceans/doc.html for

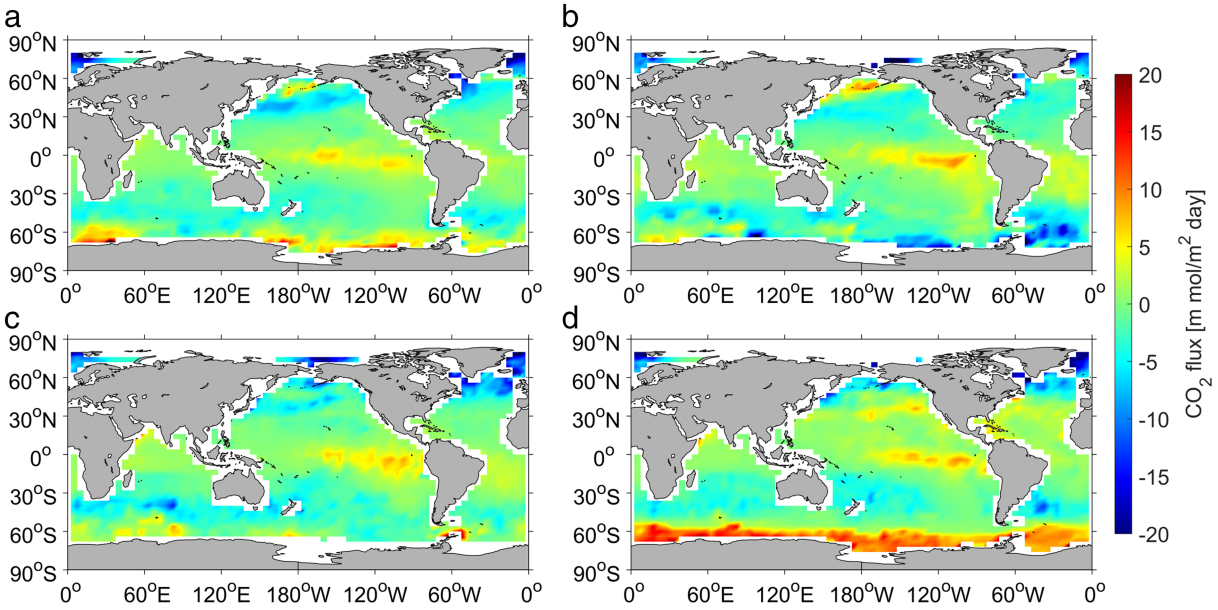

Figure 14. Estimates of global seasonal air-sea CO_2 fluxes using the ASCAT scatterometer-based transfer velocity estimates shown in Figure 13 together with monthly averaged ΔP_{CO_2} from the LDEO database NDP-094 (http://cdiac.ornl.gov/oceans/doc.html) (Takahashi et al., 2014), after rearrangement on a 4° latitude and 5° longitude grid for the Reference Year 2005. Shown are fields for (a) winter, (b) spring, (c) summer, and (d) fall.

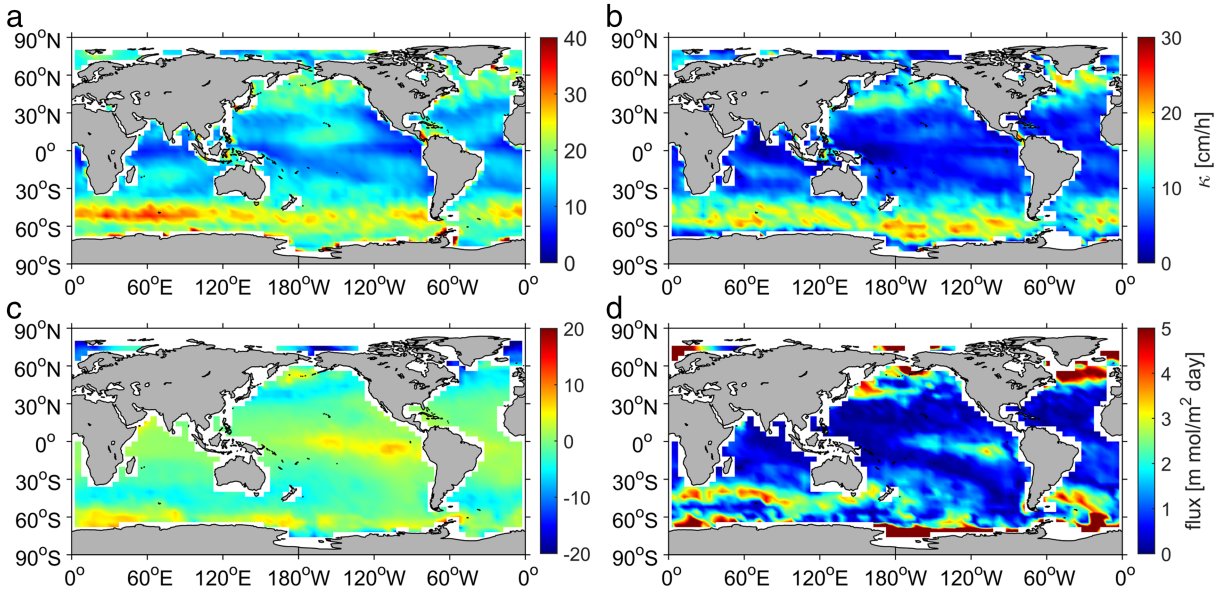

Figure 15. (left column) Time-mean of (top) air-sea CO_2 transfer velocity and (bottom) air-sea CO_2 flux from this study, averaged over Year 2012. The right column shows respective difference between our results and Wanninkhof (1992).

the Reference Year 2005. This is an updated version of Takahashi et al. (2009) representing non-El Niño years using a database of about 6.5 million P_{CO_2} data (see Takahashi et al., 2014, for details).

Figure 14 shows the resulting global seasonal scatterometer derived air-sea CO_2 flux fields. Positive values indicate the direction of the flux from the ocean into atmosphere, and negative values correspond to flux into the ocean. Compared with the wind-only parameterization, the distribution of the flux from our parameterization agrees well with the previous study of Wanninkhof (1992) for each season. The equatorial areas show

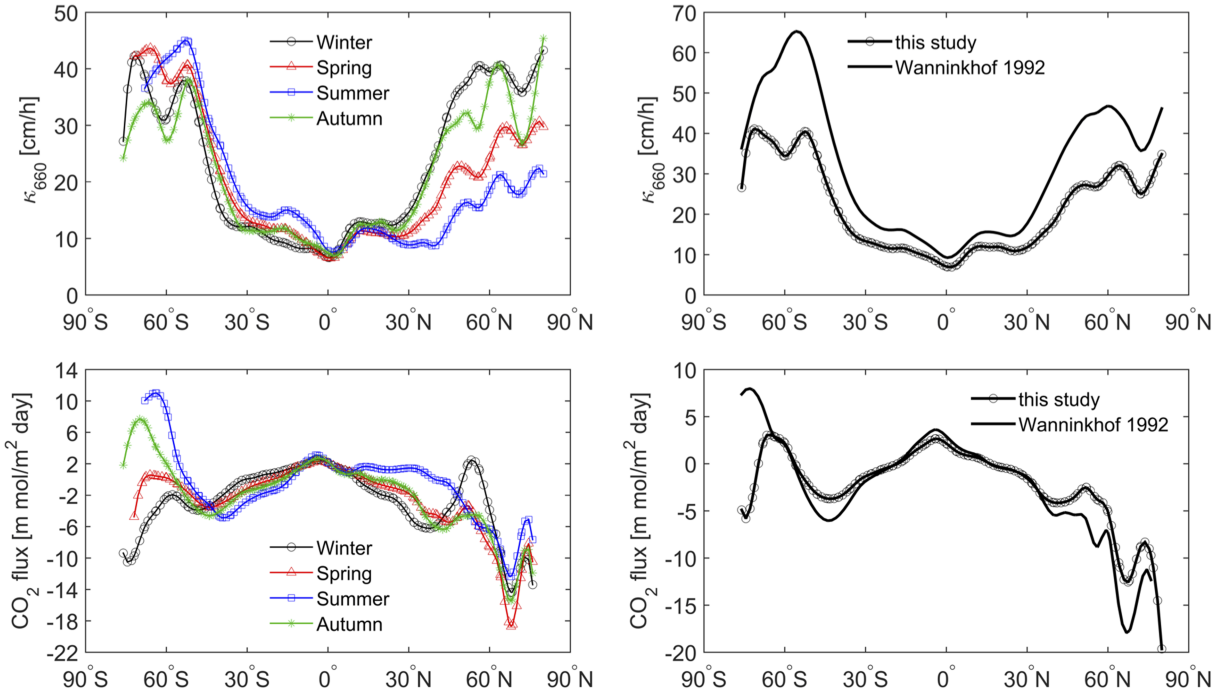

Figure 16. (left column) Zonal averages of (top) air-sea CO_2 transfer velocity and (bottom) air-sea CO_2 flux, plotted as function of latitude for individual seasons. In the right column, respective annual mean values of (top) air-sea CO_2 transfer velocity and (bottom) air-sea CO_2 flux are compared to results from Wanninkhof (1992). The transfer velocity estimates are Schmidt number corrected.

positive and higher flux than the other areas. Midlatitudes (north and south) show negative flux. Flux values are larger in high latitudes during winter and autumn as compared to the remaining seasons. However, a detailed comparison shows that, on annual averages, our estimates are smaller than that of wind-based parameterizations (see Figure 15).

Comparing results from our study with those available from Wanninkhof (1992), we find similar spatial variation but smaller values of air-sea CO_2 transfer velocity and very close values for air-sea CO_2 fluxes. The largest differences in the transfer velocity are noticed in the North Atlantic and Pacific Oceans which becomes clear in plots of zonally averaged gas transfer velocity and fluxes shown in Figure 16. In the equatorial region, the seasonal distribution of both transfer velocity and flux is similar. In the North Hemisphere, summer shows lower transfer velocity, and winter and autumn shows higher transfer velocity. Seasonal changes of gas transfer velocity in the Northern Hemisphere are larger than in the Southern Hemisphere. In 60° north, winter and autumn show strong transfer velocity near the north Pacific Currents. In the Southern Hemisphere, high seasonal variation is more around 60°. Large values of gas flux are noticed at high latitudes, over 60° north and south because of the high transfer velocity in these areas.

The strong air-sea CO_2 flux in the middle east of Pacific Ocean in the presence of small gas transfer velocity is the effect of large partial pressure differences in this area. In the tropical area, the ocean acts as a source of CO_2 because of upwelling. The North Pacific and Atlantic act as a sink of the gas flux. In the belt of 60° south, partial pressure differences control the gas flux, thereby producing high flux even though the transfer velocity is low. This area acts as a strong source of air-sea CO_2 flux.

5. Concluding Remarks

The aim of this paper was to develop an algorithm by which local scatterometer data can be used to estimate a time-varying air-sea transfer velocity κ parameterization and to apply the algorithm to actual satellite data over the global ocean. The study is based on local multifrequency and multipolarization scatterometer observations obtained in the Western Baltic. In combination with ΔP_{CO_2} measurements obtained simultaneously to the scatterometer data, we were able to develop such an algorithm and to use it to estimate surface CO_2 fluxes. The results agree with previous results using a wind speed parameterization. However, they reveal a seasonally varying coefficient to wind speed as would result from the effect of different environmental conditions on the surface roughness and air sea transfer velocity, such as wind, short waves, wave breaking, atmospheric stability, and near-surface turbulence.

The newly derived parameterization derived in the Western Baltic was applied subsequently to global monthly mean satellite-based ASCAT scatterometer fields to estimate seasonal and annual global maps of air-sea transfer velocities and CO_2 fluxes over the global ocean. We show that the new results agree in their general pattern with the previous studies using wind speed parameterization. Differences between the traditional wind-based gas transfer estimation and the new radar backscatter-gas transfer estimation were illustrated by calculating monthly averaged gas transfer velocities. In all months, the estimated gas transfer velocity using radar backscatter results in a very close value to observations with smaller root-mean-square error of 9.29 cm/hr compared to the traditional wind-based gas transfer parameterizations. A comparison reveals lower values in the backscatter-based results, especially at higher latitudes. Globally radar-based air-sea CO_2 fluxes would thereby lower by 20%.

The results presented are promising, but leave room for further improvements. Most of all, a dedicated experiment is required to extend our algorithm derived for only upwind conditions to the full spectrum of available wind directions. In that way, all satellite-based scatterometer data can be used to estimate surface CO_2 fluxes, enabling an unprecedented temporal resolution in flux data. Moreover, it needs to be investigated to what extent the algorithm derived here is biased low by using a training data set that does not represent high-wind conditions. All together, we conclude that the use of surface backscatter data to derive surface CO_2 fluxes should receive further attention than devoted to it in the past.

Acknowledgments
We thank an anonymous referee for a detailed and very constructive review. We thank M. Gade, M. Fischern, K.-W. Gurgel, and T. Schlick who all were involved in the FINO-2 measurement campaign from which data are evaluated here. Their technical support during the scatterometer measurements and data processing is gratefully acknowledged. We also thank Stefan Kern for his support and advice regarding the use of satellite data. The CO_2 flux data is provided by the Institute of Meteorology, University of Hamburg, notable F. Ament and A. Lammert. B. Schneider from the Institut für Ostseeforschung in Warnemünde provided the partial pressure of CO_2. The meteorological data from the FINO-2 platform and buoy data are provided by Bundesamt für Seeschifffahrt und Hydrographie (BSH). Scatterometer data can be made available on request through the Integrated Climate Data Center (ICDC, http://icdc.cen.uni-hamburg.de/1.html) of the Center for Earthsystem Science and Sustainability (CEN) of the Universität Hamburg authors are expected to curate the above data for at least 5 years after publication and provide a transparent process to make the data available to anyone upon request. Contribution to the DFG funded excellence cluster CliSAP of the Universität Hamburg. Funded in part through the BMBF-supported SOPRAN project.

References

Banner, M. L., & Phillips, O. (1974). On the incipient breaking of small scale waves. *Journal of Fluid Mechanics*, *65*(04), 647–656.
Bock, E. J., Hara, T., Frew, N. M., & McGillis, W. R. (1999). Relationship between air-sea gas transfer and short wind waves. *Journal of Geophysical Research*, *104*(C11), 25,821–25,831.

Broecker, H. C., Petermann, J., & Siems, W. (1978). Influence of wind on CO_2-exchange in a wind-wave tunnel, including effects of monolayers. *Journal of Marine Research*, *36*(4), 595–610.
Eumetsat, A. (2004). ASCAT calibration and validation plan. EUM/EPS/SYS/SPE/990009, 0 (0), 141.
Eumetsat, A. (2005). ASCAT level 1 product generation function specification. EUM/EPS/SYS/SPE/990009, 0 (0), 214.
Eumetsat, A. (2009a). ASCAT product guide. EUM/OPS-EPS/MAN/04/0028, 0 (0), 261.
Glover, D. M., Frew, N. M., McCue, S. J., & Bock, E. J. (2002). A multi-year time series of global gas transfer velocity from the TOPEX dual frequency, normalized radar backscatter algorithm, *Gas transfer at water surfaces* (pp. 325–331). Washington, DC: AGU.
Ho, D. T., Law, C. S., Smith, M. J., Schlosser, P., Harvey, M., & Hill, P. (2006). Measurements of air-sea gas exchange at high wind speeds in the Southern Ocean: Implications for global parameterizations. *Geophysical Research Letters*, *33*, L16611. https://doi.org/10.1029/2006GL026817
Jähne, B., Libner, P., Fischer, R., Billen, T., & Plate, E. (1989). Investigating the transfer processes across the free aqueous viscous boundary layer by the controlled flux method. *Tellus B*, *41*(2), 177–195.
Jones, W. L., & Schroeder, L. (1978). Radar backscatter from the ocean: Dependence on surface friction velocity. *Boundary-Layer Meteorology*, *13*(1-4), 133–149.
Jonsson, A., Åberg, J., Lindroth, A., & Jansson, M. (2008). Gas transfer rate and CO_2 flux between an unproductive lake and the atmosphere in northern Sweden. *Journal of Geophysical Research*, *113*, G04006. https://doi.org/10.1029/2008JG000688
Keller, W. C., Wismann, V., & Alpers, W. (1989). Tower-based measurements of the ocean C band radar backscattering cross section. *Journal of Geophysical Research*, *94*(C1), 924–930.
Kern, S., Brath, M., Fontes, R., Gade, M., Gurgel, K.-W., Kaleschke, L., et al. (2009). Multi^{3}Scat—A helicopter-based scatterometer for snow-cover and sea-ice investigations. *IEEE Geoscience and Remote Sensing Letters*, *6*(4), 703–707.
Lammert, A., & Ament, F. (2015). CO_2-flux measurements above the baltic sea at two heights: Flux gradients in the surface layer? *Earth System Science Data*, *7*(2), 311–317.
Lansø, A. S., Bendtsen, J., Christensen, J., Sørensen, L., Chen, H., Meijer, H., & Geels, C. (2015). Sensitivity of the air–sea CO_2 exchange in the Baltic Sea and Danish inner waters to atmospheric short-term variability. *Biogeosciences*, *12*(9), 2753–2772.
Liss, P. S., & Merlivat, L. (1986). Air-sea gas exchange rates: Introduction and synthesis, *The role of air-sea exchange in geochemical cycling* (pp. 113–127). Dordrecht: Springer.
Melville, W. (1996). The role of surface-wave breaking in air-sea interaction. *Annual Review of Fluid Mechanics*, *28*(1), 279–321.
Merlivat, L., & Memery, L. (1983). Gas exchange across an air-water interface: Experimental results and modeling of bubble contribution to transfer. *Journal of Geophysical Research*, *88*(C1), 707–724.
Nightingale, P. D., Liss, P. S., & Schlosser, P. (2000). Measurements of air-sea gas transfer during an open ocean algal bloom. *Geophysical Research Letters*, *27*(14), 2117–2120.
Pachauri, R. K., Allen, M. R., Barros, V. R., Broome, J., Cramer, W., Christ, R., et al. (2014). Climate change 2014: Synthesis report Contribution of Working Groups I, II and III to the fifth assessment report of the Intergovernmental Panel on Climate Change. R. Pachauri and L. Meyer (editors). Geneva, Switzerland. IPCC, 151 p., ISBN: 978-92-9169-143-2.
Plant, W., Keller, W., & Weissman, D. (1985). The dependence of the microwave radar cross section on the air-sea interaction and the wave slope, *The ocean surface* (pp. 289–296). Dordrecht: Springer.
Schneider, B., Gustafsson, E., & Sadkowiak, B. (2014). Control of the mid-summer net community production and nitrogen fixation in the central Baltic Sea: An approach based on pCO_2 measurements on a cargo ship. *Journal of Marine Systems*, *136*, 1–9.
Schneider, B., Kaitala, S., Raateoja, M., & Sadkowiak, B. (2009). A nitrogen fixation estimate for the Baltic Sea based on continuous pCO_2 measurements on a cargo ship and total nitrogen data. *Continental Shelf Research*, *29*(11), 1535–1540.
Takahashi, T., Sutherland, S. C., Chipman, D. W., Goddard, J. G., Ho, C., Newberger, T., et al. (2014). Climatological distributions of pH, pCO_2, total CO_2, alkalinity, and $CaCO_3$ saturation in the global surface ocean, and temporal changes at selected locations. *Marine Chemistry*, *164*, 95–125.
Takahashi, T., Sutherland, S. C., Sweeney, C., Poisson, A., Metzl, N., Tilbrook, B., et al. (2002). Global sea–air CO_2 flux based on climatological surface ocean pCO_2, and seasonal biological and temperature effects. *Deep Sea Research Part II: Topical Studies in Oceanography*, *49*(9), 1601–1622.
Takahashi, T., Sutherland, S. C., Wanninkhof, R., Sweeney, C., Feely, R. A., Chipman, D. W., et al. (2009). Climatological mean and decadal change in surface ocean pCO_2, and net sea–air CO_2 flux over the global oceans. *Deep Sea Research Part II: Topical Studies in Oceanography*, *56*(8), 554–577.
Wanninkhof, R. (1992). Relationship between wind speed and gas exchange over the ocean. *Journal of Geophysical Research*, *97*(C5), 7373–7382.
Wanninkhof, R., Asher, W. E., Ho, D. T., Sweeney, C., & McGillis, W. R. (2009). Advances in quantifying air-sea gas exchange and environmental forcing. *Annual Review of Marine Science*, *1*, 213–244.
Wanninkhof, R., & McGillis, W. R. (1999). A cubic relationship between air-sea CO_2 exchange and wind speed. *Geophysical Research Letters*, *26*(13), 1889–1892.
Webb, E. K., Pearman, G. I., & Leuning, R. (1980). Correction of flux measurements for density effects due to heat and water vapour transfer. *Quarterly Journal of the Royal Meteorological Society*, *106*(447), 85–100.
Weiss, A., Kuss, J., Peters, G., & Schneider, B. (2007). Evaluating transfer velocity-wind speed relationship using a long-term series of direct eddy correlation CO_2 flux measurements. *Journal of Marine Systems*, *66*(1), 130–139.
Yu, T., He, Y., Song, J., Shen, H., Wang, J., & Gao, G. (2014). Uncertainty in air–sea CO_2 flux due to transfer velocity. *International Journal of Remote Sensing*, *35*(11-12), 4340–4370.